RAPID COMMUNICATIONS

PHYSICAL REVIEW B **96**, 241409(R) (2017)

Inelastic electron tunneling mediated by a molecular quantum rotator

Toshiki Sugimoto,[1,2,*] Yuji Kunisada,[3] and Katsuyuki Fukutani[4,†]

[1]*Department of Chemistry, Graduate School of Science, Kyoto University, Kyoto 606-8502, Japan*

[2]*Precursory Research for Embryonic Science and Technology (PRESTO), Japan Science and Technology Agency (JST), Saitama 332-0012, Japan*

[3]*Center for Advanced Research of Energy and Materials, Faculty of Engineering, Hokkaido University, Hokkaido 060-8628, Japan*

[4]*Institute of Industrial Science, The University of Tokyo, Tokyo 153-8505, Japan*

(Received 30 August 2017; revised manuscript received 20 November 2017; published 21 December 2017)

Inelastic electron tunneling (IET) accompanying nuclear motion is not only of fundamental physical interest but also has strong impacts on chemical and biological processes in nature. Although excitation of rotational motion plays an important role in enhancing electric conductance at a low bias, the mechanism of rotational excitation remains veiled. Here, we present a basic theoretical framework of IET that explicitly takes into consideration quantum angular momentum, focusing on a molecular H_2 rotator trapped in a nanocavity between two metallic electrodes as a model system. It is shown that orientationally anisotropic electrode-rotator coupling is the origin of angular-momentum exchange between the electron and molecule; we found that the anisotropic coupling imposes rigorous selection rules in rotational excitation. In addition, rotational symmetry breaking induced by the anisotropic potential lifts the degeneracy of the energy level of the degenerated rotational state of the quantum rotator and tunes the threshold bias voltage that triggers rotational IET. Our theoretical results provide a paradigm for physical understanding of the rotational IET process and spectroscopy, as well as molecular-level design of electron-rotation coupling in nanoelectronics.

DOI: 10.1103/PhysRevB.96.241409

Molecule-mediated electron transport induced by electron-nuclear coupling is ubiquitous and gives a significant impact on a variety of disciplines including nanoelectronics, organic semiconductors, redox chemistry, and photosynthetic biology [1–11]. In a nanoscale molecular junction, interactions with substances such as metallic electrodes break rotational symmetry of nanoconfined molecules. Under an anisotropic potential that induces rotational-symmetry breaking, the rotational motion of a heavier molecule is hindered and converted to vibrational motion of the molecular axis around the equilibrium orientation, which is designated as frustrated rotation or librational phonon. The electron transfer mediated by excitation of such a librational phonon mode has been well understood in terms of electron-phonon coupling [5,6], contributing to developing high-performance electronic devices and inelastic electron tunneling (IET) spectroscopy that is useful for characterizing multiple properties of molecular junction.

In contrast, in the case of light molecules and functional groups, the rotational kinetic energy often exceeds the anisotropic potential energy due to the small moment of inertia for rotation [12,13]; the rotational degree of freedom is retained due to the rotational quantum effect [14–18]. It had been a long-standing issue whether electron transfer can be triggered by the excitation of rotational motion. Recent experimental studies have demonstrated that in a rotating molecular junction the electron tunneling can be enhanced accompanying rotational excitation at the respective voltage, using molecular hydrogen (H_2) and its isotopes (HD,D_2) [17,19–21] trapped between nanoelectrodes as a model system of molecular rotator [22–28]. It was also shown that the rotational motion can be probed through IET spectroscopy combined with scanning tunneling microscopy (STM) [22–28]. Despite the intensive studies, however, a molecular-level mechanism of rotational IET has been unclear due to the inherent difficulty in treating the wave function and angular momentum of rotating H_2 molecules in the existing theory of IET based on the electron-phonon coupling [29–32]. To clarify the mechanism of rotational IET process in the H_2 junctions, we present a basic theoretical framework that explicitly takes into consideration quantum angular momentum. This Rapid Communication demonstrates that the orientationally anisotropic character of the electrode-rotator coupling imposes rigorous rotational selection rules in rotational excitations. In addition, we show that the rotational symmetry breaking induced by the anisotropic potential is the key factor that tunes the rotational-energy structure of the spatially confined quantum rotator. Our theoretical results describe well the experimental results reported previously [22–28].

The interaction between a rotating molecule and neighboring electrodes is generally weak [17,19]. Therefore, in the case of weakly coupled molecular junctions [33,34], the unperturbed Hamiltonian $\hat{H}^{(0)}$ for the system is taken as $\hat{H}^{(0)} = \hat{H}_T^{(0)} + \hat{H}_M^{(0)} + \hat{H}_S^{(0)}$, where $\hat{H}_T^{(0)}$, $\hat{H}_M^{(0)}$, and $\hat{H}_S^{(0)}$ are the Hamiltonians of the isolated state of the STM tip, rotating molecule, and substrate, respectively [Fig. 1(a)]; the perturbative interaction $\widehat{U}$ is taken as $\widehat{U} = \widehat{U}_{\mathrm{TM}} + \widehat{U}_{\mathrm{MS}}$, where $\widehat{U}_{\mathrm{TM}}$ and $\widehat{U}_{\mathrm{MS}}$ represent Coulomb-interaction operators that are composed of one-electron attractive terms and two-electron repulsive terms between the STM tip and rotating molecule, and the molecule and substrate, respectively. For simplicity, we assume one-level approximation where a single electronic level of the rotating molecule is coupled to an electronic level of two metallic electrodes. The tunneling current $I(V)$

*Corresponding author: toshiki@kuchem.kyoto-u.ac.jp

†Corresponding author: fukutani@iis.u-tokyo.ac.jp

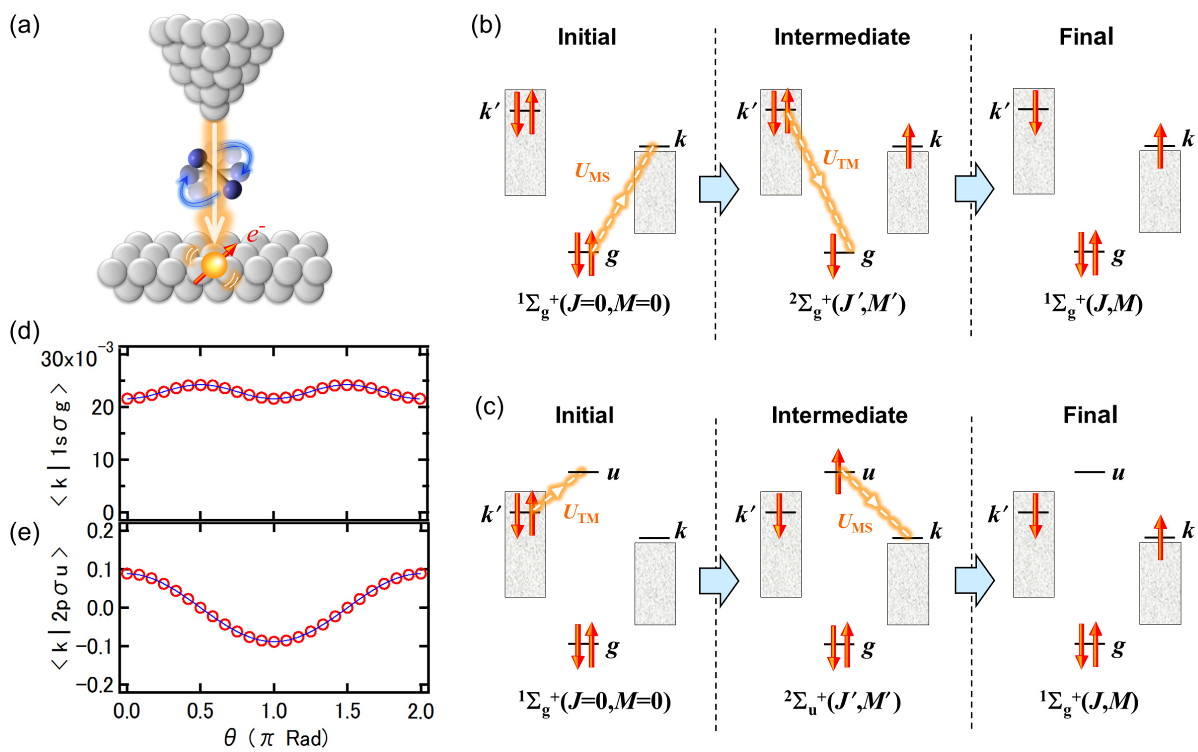

FIG. 1. IET mechanism mediated by rotational excitation of H_2 weakly trapped within nanoscale junction. (a) Schematic illustration of rotational excitation of H_2 via IET from STM tip to metal electrode. (b) and (c) Electronic structure diagrams of IET processes from a metal electrode (k' orbital) to another electrode (k orbital) mediated by (b) *para*-H_2^+ in the $^2\Sigma_g{}^+$ state and (c) *para*-H_2^- in the $^2\Sigma_u{}^+$ state. (d) and (e) Typical θ dependence of overlap integral between (d) k and g, and (e) k and u (Supplemental Material Sec. 2 [35]). Solid lines are results of curve fitting with (d) a linear combination of $P_0(\cos\theta)$ and $P_2(\cos\theta)$, and (e) $P_1(\cos\theta)$.

is described as [5]

$$I(V) = e\frac{2\pi}{\hbar}\sum_{f,i} f(\varepsilon_i)[1 - f(\varepsilon_f + eV)]\,\delta(\varepsilon_f + \Delta E_{\mathrm{rot}} - \varepsilon_i) \times \left|\sum_m \frac{\langle f|\widehat{U}|m\rangle\langle m|\widehat{U}|i\rangle}{\varepsilon_m - \varepsilon_i - i0}\right|^2, \tag{1}$$

where e, V, and $\hbar$ are the elementary charge, applied voltage, and the reduced Plank constant, respectively; ε_i,ε_m, and ε_f are the electronic energies of the initial, intermediate, and final states, respectively; ΔE_{rot} is the energy needed for rotational excitation; $f(\varepsilon)$ is the Fermi-Dirac distribution function relative to the Fermi level of the STM tip; and $i0$ denotes an infinitesimal positive imaginary part. Because $\varepsilon_f = \varepsilon_i - \Delta E_{\mathrm{rot}}$, the zero-temperature and low-bias approximation [29] gives the tunneling conductance as

$$\frac{\partial I}{\partial V} \propto |\widehat{U}_{fm}\widehat{U}_{mi}|^2\left|\int d\varepsilon_m \frac{D_{\mathrm{M}}(\varepsilon_m)}{\varepsilon_m - (\bar{E}_F + \Delta E_{\mathrm{rot}}) - i0}\right|^2 \times D_{\mathrm{T}}(\bar{E}_F + \Delta E_{\mathrm{rot}})\,D_{\mathrm{S}}(\bar{E}_F)\,\Theta(eV - \Delta E_{\mathrm{rot}}), \tag{2}$$

where $D_{\mathrm{T}}, D_{\mathrm{M}}$, and D_{S} denote the electron densities of states (DOS) of the STM tip, molecule and substrate, respectively (see Fig. S1 in the Supplemental Material [35]); Θ is the step function; E_{F} and $\bar{E}_{\mathrm{F}} \equiv E_{\mathrm{F}} - eV$ are the Fermi level of the STM tip and the substrate, respectively; and $\widehat{U}_{mi}$ and $\widehat{U}_{fm}$ are the matrix elements of $\widehat{U}$ representing electron hopping. $\Delta E_{\mathrm{rot}}/e$ corresponds to the threshold bias voltage of the IET process. Electron transfer is induced by the second-order coupling matrix element $\widehat{U}_{fm}\widehat{U}_{mi} = (\widehat{U}_{\mathrm{TM}} + \widehat{U}_{\mathrm{MS}})_{fm}(\widehat{U}_{\mathrm{TM}} + \widehat{U}_{\mathrm{MS}})_{mi}$. There are two possible channels as schematically shown in Figs. 1(b), 1(c), and S1: $(\widehat{U}_{\mathrm{TM}})_{fm}(\widehat{U}_{\mathrm{MS}})_{mi}$ and $(\widehat{U}_{\mathrm{MS}})_{fm}(\widehat{U}_{\mathrm{TM}})_{mi}$ terms describe the electron tunneling processes mediated by the positive ion and negative ion, respectively. In the following, we focus on a quantum-rotator junction that contains a H_2 molecule as a model system.

For the IET process mediated by positive ion (H_2^+), the wave functions for the initial, intermediate, and final states are given by a product of the electronic and rotational parts as $\Psi_i = |k'\bar{k}'g\bar{g}|Y_{00}$, $\sqrt{2}\Psi_m^+ = |k'\bar{k}'(g\bar{k} - \bar{g}k)|Y_{J'M'}$, and $\sqrt{2}\Psi_f = |g\bar{g}(k'\bar{k} - \bar{k}'k)|Y_{JM}$, respectively [Fig. 1(b)], where $Y_{J,M}$ is a spherical-harmonic function with rotational quantum number J and its z component M; k' and k are the one-electron spin orbitals of the surface Bloch state below E_{F} of the STM tip and above $\bar{E}_{\mathrm{F}}$ of the metal substrate, respectively; g is the $1s\sigma_g$ spin orbital of H_2. The spin orbitals with and without an overbar indicate up-spin and down-spin orbitals, respectively. There is no resonant molecular ionic state close to the Fermi level of the substrate [Fig. S1(a)], indicating that the electron-rotation coupling discussed below is induced by the electronically nonresonant process. It is instructive to discuss the rotational excitation channel from the rotational ground state of *para*-H_2

(Table S1; see also Supplemental Material Sec. 4 [35]) in the case where k' and k have the σ azimuthal rotational symmetry around the tip-substrate axis such as s, p_z, and d_z^2, because the wave function of the tip and substrate atoms without σ azimuthal rotational symmetry has a small electron density derived from the node along the tip-substrate axis, making only a small contribution to the tunneling current [36] (see Supplemental Material Sec. 3 for rotational selection rules of other special cases [35]). Note that the electron-transfer probability between H_2 and the electrodes depends on θ. Due to the *gerade* inversion symmetry in the molecular coordinate derived from the even parity of electron orbital, the molecular $1s\sigma_g$ orbital has the twofold symmetry with respect to θ in the laboratory coordinate. This indicates that both electron overlap integrals $\langle k\,|g\rangle_{\rm el}$ and $\langle k'\,|g\rangle_{\rm el}$ have a rotational periodicity of π [Figs. 1(d) and S2]. These overlap integrals do not depend on azimuthal angle φ due to the σ azimuthal rotational symmetry of the k and k' orbitals. Thus, they are typically expanded in the Legendre polynomials of zero and second degrees as a function of cosθ, i.e., $C_0P_0(\cos\theta) + C_2P_2(\cos\theta)$; the contribution of the Legendre polynomials of odd degree is strictly excluded by the gerade symmetry. Given that the electronic couplings $(\widehat{U}_{\rm MS})_{mi}$ and $(\widehat{U}_{\rm TM})_{fm}$ are roughly proportional to the orbital overlap [17,37,38], the $(\widehat{U}_{\rm MS})_{mi}$ and $(\widehat{U}_{\rm TM})_{fm}$ terms are described as

$$\langle\Psi_m^+|\hat{U}_{\rm MS}\,|\Psi_i\,\rangle \propto \langle Y_{J'M'}|\,\langle k\,|g\rangle_{\rm el}|Y_{00}\rangle$$
$$\approx \langle Y_{J'M'}|\,C_0P_0 + C_2P_2|Y_{00}\rangle, \tag{3}$$

$$\langle\Psi_f|\,\hat{U}_{\rm TM}\,|\,\Psi_m^+\,\rangle \propto \langle Y_{JM}|\,\langle g\,|k'\rangle_{\rm el}|Y_{J'M'}\rangle$$
$$\approx \langle Y_{JM}|\,C_0'P_0 + C_2'P_2|Y_{J'M'}\rangle. \tag{4}$$

Since the rotational integral $\langle Y_{J'M'}|\,P_2(\cos\theta)\,|Y_{00}\rangle$ is nonzero for $J'=2$ and $M'=0$, $\langle Y_{JM}|\,P_2(\cos\theta)\,|Y_{J'M'}\rangle$ is nonzero for $J=0$, 2, and 4 and $M=0$. The isotropic electrode-rotator coupling terms only contribute to the elastic process with $\Delta J=0$ and $\Delta M=0$. We emphasize here that it is the anisotropic electrode-rotator coupling, i.e., angle-dependent tunneling amplitude, that induces rotational excitation in the IET process [11]. Because the contribution of the $C_0P_0(\cos\theta)$ term is much larger than that of the $C_2P_2(\cos\theta)$ term [Fig. 1(d)] and thus the values of $C_0'C_2$, C_0C_2', and $C_0'C_2$ are about one order of magnitude larger than that of C_2C_2' (Table S4), the IET process accompanying the $\Delta J=+4$ rotational excitation is negligible compared with the $\Delta J=+2$ rotational excitation process.

Similarly, in the case of the negative-ion ($H_2{}^-$)-mediated IET process described by the $(\widehat{U}_{\rm MS})_{fm}(\widehat{U}_{\rm TM})_{mi}$ term [Fig. 1(c)], the wave function for the intermediate state is given by $\sqrt{2}\Psi_m^- = |\,g\bar{g}(k'\bar{u} - \bar{k}'u)\,|Y_{J'M'}$, where u is the $2p\sigma_u$ molecular spin orbital. Although the electron DOS of the $H_2{}^-$ state is rather broadened [Fig. S1(b)], the contribution of resonant electron transfer is still negligibly small (Supplemental Material Sec. 2 [35]). Due to the *ungerade* inversion symmetry derived from the odd parity of the $2p\sigma_u$ orbital in the molecular coordinate, the electronic overlap integrals $\langle k\,|u\rangle_{\rm el}$ and $\langle k'\,|u\rangle_{\rm el}$ are antisymmetric with respect to π rotation and have a rotational periodicity of 2π [Figs. 1(e) and S2]. Therefore, they are typically expanded in the Legendre polynomials of first degree as a function of cosθ, i.e., $C_1P_1(\cos\theta)$; the contribution of the Legendre polynomials of even degree is strictly excluded by the ungerade symmetry. The $(\widehat{U}_{\rm TM})_{mi}$ and $(\widehat{U}_{\rm MS})_{fm}$ terms are thus described as

$$\langle\Psi_m^-|\,\hat{U}_{\rm TM}\,|\,\Psi_i\,\rangle \propto \langle Y_{J'M'}|\langle u\,|k'\rangle_{\rm el}|Y_{00}\rangle$$
$$\approx \langle Y_{J'M'}|\,C_1P_1(\cos\theta)|Y_{00}\rangle, \tag{5}$$

$$\langle\Psi_f|\,\hat{U}_{\rm MS}\,|\,\Psi_m^-\,\rangle \propto \langle Y_{JM}|\,\langle k\,|u\rangle_{\rm el}|Y_{J'M'}\rangle$$
$$\approx \langle Y_{JM}|\,C_1'P_1(\cos\theta)\,|Y_{J'M'}\rangle. \tag{6}$$

The rotational integrals $\langle Y_{J'M'}|\,P_1(\cos\theta)|Y_{00}\rangle$ and $\langle Y_{JM}|P_1(\cos\theta)\,|Y_{J'M'}\rangle$ are nonzero for $J'=1$ and $M'=0$, and $J=0{,}2$ and $M=0$, respectively, indicating that the rotational excitation channel for IET mediated by the $H_2{}^-$ is $\Delta J=2$ and $\Delta M=0$. In this case, there is no contribution of isotropic electrode-rotator coupling, and the elastic tunneling process is also induced by anisotropic electrode-rotator coupling via the $J'=1$ and $J-J'=-1$ path.

The rotational selection rules of IET are concluded to be $\Delta J=2$ and $\Delta M=0$ for both processes mediated by positive and negative H_2 ions. Note that all electron-transfer steps from initial to intermediate states and intermediate to final states [Figs. 1(b) and 1(c)] satisfy the strict restriction with respect to the possible rotational state of *para*-H_2: the rotational quantum number of *para*-H_2 in the electronic Σ_u^+ states is odd, while that in the electronic ${}^2\Sigma_g{}^+$ states is even (Table S1). Because the value of $|C_1C_1'|^2$ for $2p\sigma_u$ is about two orders of magnitude larger than that of $|C_0C_2'|^2$ and $|C_0'C_2|^2$ for $1s\sigma_g$ (Table S4), the contribution of the $H_2{}^-$-mediated IET is more than two orders of magnitude larger than that of the H_2^+-mediated IET (Supplemental Material Sec. 4 [35]).

Isotope effects on the rotational selection rules are worth discussing. In the case of the D_2 molecule that consists of two identical nuclei and has inversion symmetry, the rotational selection rules are strictly the same as those of H_2. In the case of the HD molecule, the electronic orbitals are classified into gerade or ungerade symmetry as H_2 within the adiabatic approximation. When the nuclear motion is taken into account, however, the gerade and ungerade electronic orbitals are partially mixed due to the nonadiabatic effect [39,40]. The electron-transfer matrix elements $(\widehat{U}_{\rm TM})_{mi}$ and $(\widehat{U}_{\rm MS})_{fm}$ in the HD$^-$-mediated tunneling process are thus given as $C_1P_1 + C_0P_0 + C_2P_2$ and $C_1'P_1 + C_0'P_0 + C_2'P_2$, respectively, resulting in the selection rules of $\Delta J = 1{,}2{,}3{,}4$ and $\Delta M=0$ for rotational IET. However, because the nonadiabatic gerade-ungerade mixing is as small as 10^{-2} in the HD molecule [39,40], the contribution of P_0 and P_2 terms in the HD$^-$-mediated tunneling is negligibly small ($C_0/C_1 \sim 10^{-2}, C_2/C_1 \sim 10^{-3}$). Therefore, the same rotational selection rules as the H_2 molecule, $\Delta J=2$ and $\Delta M=0$, are also operative in the HD junction. Our result validates the previous experimental observation for HD junctions that the $\Delta J=1$ transition channel was negligibly small compared with the $\Delta J=2$ [24,25].

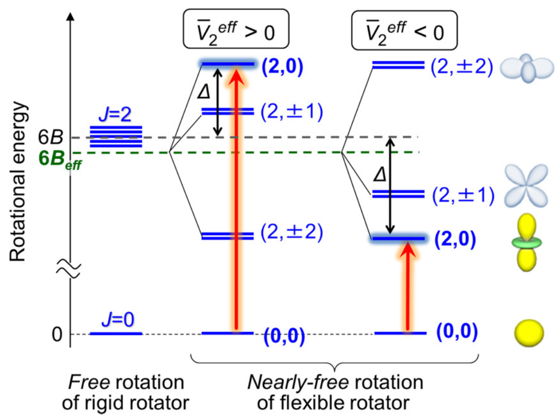

FIG. 2. Rotational-energy-level splitting of *para*-H_2 under an anisotropic potential. The rotational transition from $(J,M) = (0,0)$ state to (2,0) state is indicated by red arrows. See the main text for nomenclatural details.

To give a molecular-level insight into the threshold bias voltage of the rotational IET process, rotational-energy structure of the quantum rotator should be discussed. In the nanoscale junction, not only the potential energy V but also the equilibrium intramolecular bond distance R_e of H_2 changes periodically with θ due to the anisotropic electrode-molecule interaction that breaks rotational symmetry in the *free rotation*. In this case, the traditional *free rigid rotator* model as well as the *nearly-free rigid rotator* model [12,19–21] assuming constant R_e seems inappropriate; the rotational motion of H_2 in the junction would be better described by the *nearly-free flexible-rotator* model in which R_e anisotropically deviates from the gas-phase value R_{eg} depending on θ (see Supplemental Material Sec. 5 [35] for details). Owing to the symmetry breaking in the free gas phase and the resultant twofold rotational symmetry of the H_2 junction with respect to θ, the potential energy and the deviation of R_e from R_{eg} are expressed by the Legendre polynomials of even degree as $V(\theta) = V_0 + V_2 P_2(\cos\theta)$ and $\Delta R_e \equiv R_e - R_{eg} \approx \Delta R_{e0} + \Delta R_{e2} P_2(\cos\theta)$ where V_0 and ΔR_{e0} are isotropic contribution, and V_2 and ΔR_{e2} are anisotropic contribution. The dependence of V and ΔR_e on the azimuthal angle φ is negligibly small for the weakly trapped H_2 (Fig. S6) [18,21,41]. The Schrödinger equation of the nearly-free *flexible rotator* is thus described by Eq. (S14): $[B^{\rm eff}\hat{J}^2 + \bar{V}_2^{\rm eff} P_2(\cos\theta)]\,\psi_{\rm rot} = E_{\rm rot}\psi_{\rm rot}$, where $B^{\rm eff} \equiv B[1 - 2(\Delta\bar{R}_{e0}/R_{eg})]$ is the effective rotational constant and $\bar{V}_2^{\rm eff} = \bar{V}_2 - 2B\hat{J}^2(\Delta\bar{R}_{e2}/R_{eg})$ is the effective potential anisotropy (see Supplemental Material Sec. 5 [35] for details). Within the first-order perturbation theory using zero-order wave functions in the isolated states, the rotational energy of the nearly-free *flexible rotator* is given as $E_{\rm rot} = \langle Y_{J,M}|B^{\rm eff}\hat{J}^2 + \bar{V}_2^{\rm eff} P_2(\cos\theta)|Y_{J,M}\rangle$. Therefore, the rotational-energy shift from the gas-phase value $BJ(J+1)$ is described as

$$\Delta E_{\rm rot}(J,M) = -2BJ(J+1)(\Delta\bar{R}_{e0}/R_{eg}) + \bar{V}_2^{\rm eff}(J)\langle Y_{J,M}|P_2(\cos\theta)|Y_{J,M}\rangle, \quad (7)$$

where $B \equiv \hbar^2/2\mu R_{eg}^2$ is the rotational constant of H_2 in the gas phase, $\bar{V}_2^{\rm eff}(J) = \bar{V}_2 - 2BJ(J+1)(\Delta\bar{R}_{e2}/R_{eg})$ is the effective potential anisotropy, and the horizontal bars indicate mean values with respect to the center-of-mass position z of H_2 (Fig. 3). Equations (7) and (S17) indicate that the degenerated rotational levels of $J = 2$ in the gas phase are split by the rotational symmetry breaking induced by anisotropy $\bar{V}_2^{\rm eff}(J)$. The resultant total energy shifts of the $(J,M) = (0,0)$, (2,0), (2, ±1), and (2, ±2) states are 0, $-12B(\Delta\bar{R}_{e0}/R_{eg}) + (2/7)\bar{V}_2^{\rm eff}(2)$, $-12B(\Delta\bar{R}_{e0}/R_{eg}) + (1/7)\bar{V}_2^{\rm eff}(2)$, and $-12B(\Delta\bar{R}_{e0}/R_{eg}) - (2/7)\bar{V}_2^{\rm eff}(2)$, respectively (Fig. 2).

To quantitatively evaluate rotational-energy structure, we have performed spin-polarized density-functional theory (DFT) calculations for H_2 between the Au(110) electrode and STM tip by taking account of the van der Waals interaction (Supplemental Material Secs. 6 and 11 [35]). The values of V and ΔR_e were derived as a function of z for particular θ and φ and the distance between the STM tip and Au(110), d. Figure S6 shows that the azimuthal-angle dependence is negligibly small, indicating that H_2 in the junction has azimuthal rotational symmetry; this is because the corrugation of the electronic wave functions of Au(110) and the STM tip is smoothened at a rather distant z [18,21,41]. Given that only the $\Delta M = 0$ channel is allowed in the rotational IET process, the threshold energy relative to the gas-phase value $6B$ is $\Delta E_{\rm rot}(2,0) = -12B(\Delta\bar{R}_{e0}/R_{eg}) + (2/7)\bar{V}_2^{\rm eff}(2)$.

Figure 3 shows the isotropic and anisotropic contributions of V and ΔR_e at $d = 20$, 7.5, and 7.0 Å as a function of z (Supplemental Material Sec. 7 [35]). At $d = 20$ Å, H_2 interacts only with Au(110). The mean position $\bar{z}$ of H_2 for the ground state in V_0 potential is $\bar{z} \sim 3.2$ Å [Figs. 3(a) and S7(a)]. $\bar{V}_2$, $\Delta\bar{R}_{e0}/R_{eg}$, and $\Delta\bar{R}_{e2}/R_{eg}$ are -2.6 meV, 2.8×10^{-3}, and 2.7×10^{-3}, respectively [Table I]. The negative sign of $\bar{V}_2$ indicates that H_2 on Au(110) prefers perpendicular orientation; the $M = 0$ rotational state is the most stable (Fig. 2). The value of $\bar{V}_2 = -2.6$ meV is consistent with the values on other noble metal surfaces of Cu and Ag [15,20,21,41]. When the STM tip approaches the Au(110) electrode, the center-of-mass position of H_2 in the V_0 potential is rather delocalized between $3.0 \leqslant z \leqslant 5.0$ Å at $d = 7.5$ Å and $3.0 \leqslant z \leqslant 4.5$ Å at $d = 7.0$ Å due to the additional attractive interaction with the STM tip [Figs. 3(b) and 3(c)]. As d decreases, both the isotropic and anisotropic potentials become deeper and $\Delta R_{e0}/R_{eg}$ and $\Delta R_{e2}/R_{eg}$ increase owing to the partial hybridization interaction of the antibonding H_2 molecular orbital [21,41] with the Au(110) and STM-tip surface orbitals. Values of $\bar{V}_2$, $\Delta\bar{R}_{e0}/R_{eg}$, and $\Delta\bar{R}_{e2}/R_{eg}$ are shown in Table I. The rotational-energy shifts derived from the first term of Eq. (7), $6B_{\rm eff} - 6B = -12B(\Delta\bar{R}_{e0}/R_{eg})$, are -0.25, -0.13, and -0.35 meV at $d = 20$, 7.5, and 7.0 Å, respectively, while those derived from the second term of Eq. (7), $(2/7)\bar{V}_2^{\rm eff}(2)$, are -0.69, -1.1, and -2.0 meV at $d = 20$, 7.5, and 7.0 Å, respectively (Table I). Therefore, the total rotational-energy shifts $\Delta E_{\rm rot}(2,0)$ are -0.9, -1.2, and -2.4 meV at $d = 20$, 7.5, and 7.0 Å, respectively; the results are in good agreement with the rotational-energy shifts at $d = 7.5$ and 7.0 Å (Table I) observed in the previous IET experiment [24]. Considering the contribution of $\bar{V}_2$, $6B_{\rm eff} - 6B \propto \Delta\bar{R}_{e0}/\bar{R}_{eg}$, and $\bar{V}_2 - \bar{V}_2^{\rm eff} \propto \Delta\bar{R}_{e2}/\bar{R}_{eg}$ on the rotational-energy shift (Table I), i.e., $|\bar{V}_2|$ (anisotropic potential

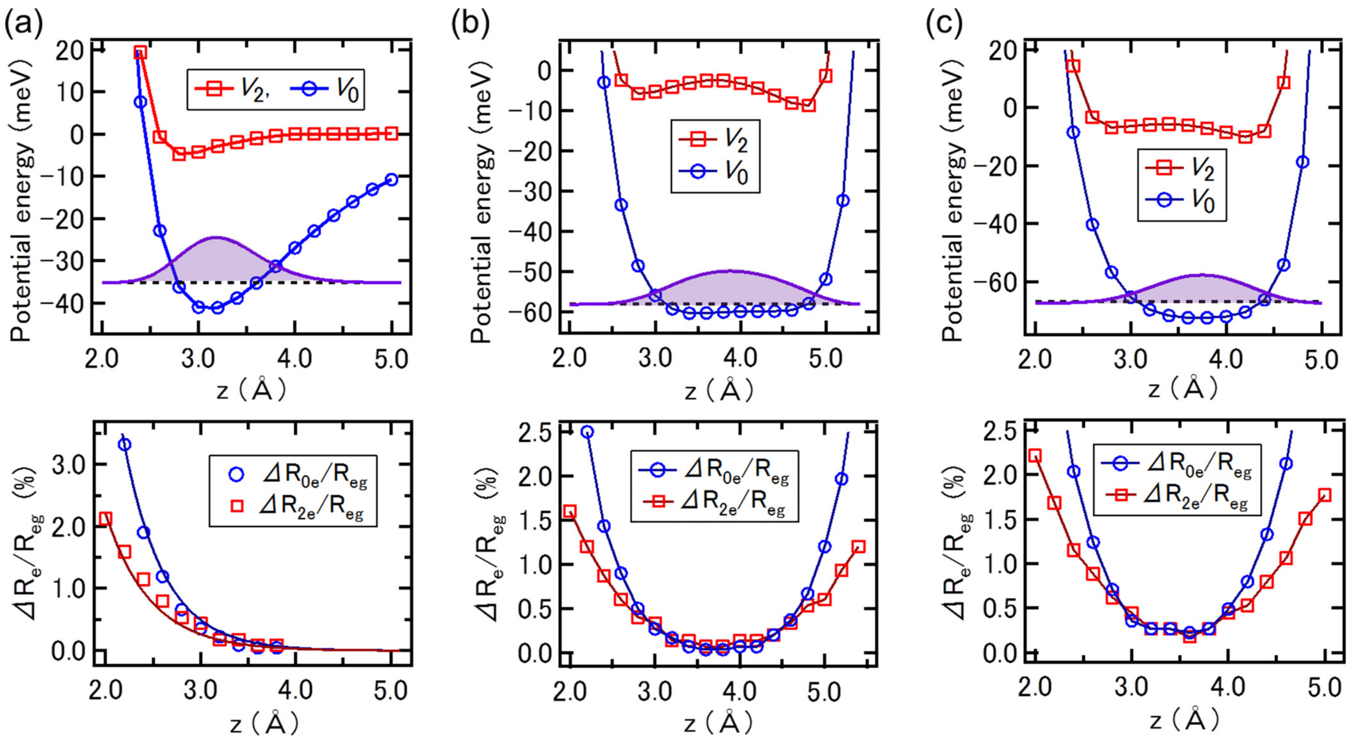

FIG. 3. Calculated values of $V_0, V_2, \Delta R_{e0}$, and ΔR_{e2} for a H_2 molecule trapped between the STM tip and Au(110) as a function of center-of-mass position z. Tip-Au(110) distance d is (a) 20 Å, (b) 7.5 Å, and (c) 7.0 Å. Both H_2 and the STM tip are at an on-top site of Au(110) (see also Supplemental Material Secs. 6, 7, and 11 for details [35]).

effect) $\gg |6B_{\text{eff}} - 6B|$ (isotropic kinetic effect) $\gg |\bar{V}_2 - \bar{V}_2^{\text{eff}}|$ (anisotropic kinetic effect), it can be concluded that the rotational-energy structure of H_2 in the nanoscale junction is dominated by the *potential anisotropy* $\bar{V}_2$, in contrast to the conventional assumption in the previous rotational IET spectroscopy [24–28] that H_2 is *freely* rotating in the nanoscale junction and the rotational-energy shift is dominated by the changes in the isotropic rotational kinetic energy $6B_{\text{eff}} - 6B \propto \Delta\bar{R}_{e0}/R_{eg}$. As discussed in Supplemental Material Sec. 9 [35], the contribution of the static quadrupole interaction with the electric-field gradient is also negligibly small for the rotational-energy structure.

Finally, our theoretical framework is applicable to other quantum-rotator systems. For example, in the case of two H_2 rotators simultaneously trapped in a nanoscale junction, we found that the rotational excitation energy of the two H_2 molecules also varies as a function of tip-substrate distance due to the anisotropic confinement (Fig. S9). Sequential rotational transitions of (i) two *para*-H_2 ($J = 0 \rightarrow 2$), (ii) *para*-H_2 ($J = 0 \rightarrow 2$) and *ortho*-H_2 ($J = 1 \rightarrow 3$), and (iii) two *ortho*-H_2 ($J = 1 \rightarrow 3$), within a nanoscale junction (Supplemental Material Sec. 10 [35]) validate the unidentified threshold voltage of IET [22] at around 90, 120, and 150 mV, respectively.

In summary, the microscopic mechanism of electron tunneling accompanying quantum rotation is demonstrated theoretically. We found that the isotropic coupling cannot contribute to the rotational IET process; this process is exclusively induced by the θ-dependent tunneling amplitude derived from the anisotropic character of the short-range electrode-rotator coupling. Only the specific transfer channel that adequately exchanges a quantum angular momentum between the electronic orbital and molecular rotational degrees of freedom is allowed. Using first-principles calculation, we also show that the *potential anisotropy* that induces rotational symmetry breaking dominates the rotational-energy structure of the spatially confined quantum rotator between electrodes; thus the threshold bias voltage that triggers the rotational IET process is sensitively tuned by the size of nanocavity between electrodes via *potential anisotropy*.

TABLE I. Calculated values of structure parameter, potential anisotropy, and the resultant contribution of kinetic and potential energy on rotational-energy shift of H_2 at typical tip-Au(110) distance d. Experimentally observed rotational-energy shifts [26] are also shown for comparison

d (Å)	$\Delta\bar{R}_{e0}/R_{eg}$	$\Delta\bar{R}_{e2}/R_{eg}$	$6B_{\text{eff}} - 6B$ (meV)	$\bar{V}_2$ (meV)	$\bar{V}_{\text{eff}}^{J=2}$	$(2/7)\bar{V}_{\text{eff}}^{J=2}$ (meV)	$\Delta E_{\text{rot}}^{NF}(2,0)$ (meV)	Observed shift (meV)
20.0	2.8×10^{-3}	2.7×10^{-3}	-2.5×10^{-1}	−2.6	−2.4	-6.9×10^{-1}	-9.4×10^{-1}	
7.5	1.5×10^{-3}	1.2×10^{-3}	-1.3×10^{-1}	−3.8	−3.7	−1.1	−1.2	-0.9 ± 0.4
7.0	4.0×10^{-3}	3.3×10^{-3}	-3.5×10^{-1}	−7.1	−6.9	−2.0	−2.4	-2.7 ± 0.2

We are grateful to Kuniyuki Miwa, Hiromu Ueba, Kazuya Watanabe, and Yoshiyasu Matsumoto for fruitful discussions. This work was supported by MEXT KAKENHI: Grant-in-Aid for Scientific Research on Innovative Areas, Grants No. 16H00937 and No. 16H00928; JSPS KAKENHI: Grant-in-Aid for Young Scientists (A), Grant No. 16H06029; Grant-in-Aid for Specially Promoted Research, Grant No. 17H06087; Grant-in-Aid for Young Scientists (B), Grant No. 17K14114; and Grant-in-Aid for Scientific Research (A), Grant No. 17H01057.

[1] R. H. M. Smit, Y. Noat, C. Untiedt, N. D. Lang, M. C. van Hemert, and J. M. van Ruitenbeek, Measurement of the conductance of a hydrogen molecule, Nature (London) **419**, 906 (2002).
[2] W. H. A. Thijssen, D. Djukic, D. A. F. Otte, R. H. Bremmer, and J. M. Ruitenbeek, Vibrationally Induced Two-Level Systems in Single-Molecule Junctions, Phys. Rev. Lett. **97**, 226806 (2006).
[3] S. Aradhya and L. Venkataraman, Single-molecule junctions beyond electronic transport, Nat. Nanotechnol. **8**, 399 (2013).
[4] E. Maggio and A. Troisi, An expression for the bridge-mediated electron transfer rate in dye-sensitized solar cells, Philos. Trans. R. Soc. A **372**, 20130011 (2014).
[5] A. Nitzan, *Chemical Dynamics in Condensed Phases* (Oxford University Press, New York, 2006).
[6] K.-I. Inoue, K. Watanabe, T. Sugimoto, Y. Matsumoto, and T. Yasuike, Disentangling Multidimensional Nonequilibrium Dynamics of Adsorbates: CO Desorption from Cu(100), Phys. Rev. Lett. **117**, 186101 (2016).
[7] K. Miyata, Y. Kurashige, K. Watanabe, T. Sugimoto, S. Takahashi, S. Tanaka, J. Takeya, T. Yanai, and Y. Matsumoto, Coherent singlet fission activated by symmetry breaking, Nat. Chem. **9**, 983 (2017).
[8] R. A. Marcus, Electron transfer reactions in chemistry. Theory and experiment, Rev. Mod. Phys. **65**, 599 (1993).
[9] K. Shirai, T. Sugimoto, K. Watanabe, M. Haruta, H. Kurata, and Y. Matsumoto, Effect of water adsorption on carrier trapping dynamics at the surface of anatase TiO_2 nanoparticles, Nano Lett. **16**, 1323 (2016).
[10] F. D. Lewis and Y. Wu, Dynamics of superexchange photoinduced electron transfer in duplex DNA, J. Photochem. Photobiol., C **2**, 1 (2001).
[11] J. Schaffert, M. C. Cottin, A. Sonntag, C. A. Bobisch, R. Möller, J.-P. Gauyacq, and N. Lorente, Tunneling electron induced rotation of a copper phthalocyanine molecule on Cu(111), Phys. Rev. B **88**, 075410 (2013).
[12] T. B. Macrury and J. R. Sams, Hindered rotation of adsorbed diatomic molecules I. Eigenvalues and eigenstates of hindered rotator, Mol. Phys. **19**, 337 (1970).
[13] T. Sugimoto and K. Fukutani, Electric-field-induced nuclear-spin flips mediated by enhanced spin–orbit coupling, Nat. Phys. **7**, 307 (2011).
[14] S. Andersson and J. Harris, Observation of Rotational Transitions for H_2, D_2, and HD Adsorbed on Cu(100), Phys. Rev. Lett. **48**, 545 (1982).
[15] A. J. Berlinsky, Rotational excitation of physisorbed H_2 by low-energy electron scattering, Phys. Rev. B **26**, 443(R) (1982).
[16] K. Svensson and S. Andersson, Rotational spectra of physisorption hydrogen, Surf. Sci. **392**, L40 (1997).
[17] E. Ilisca, o-pH_2conversion on noble metals, J. Phys. I (France) **1**, 1785 (1991).
[18] K. Svensson, Two-Dimensional Quantum Rotation of Adsorbed H_2, Phys. Rev. Lett. **83**, 124 (1999).
[19] K. Fukutani and T. Sugimoto, Physisorption and ortho-para conversion of molecular hydrogen on solid surfaces, Prog. Surf. Sci. **88**, 279 (2013).
[20] T. Sugimoto and K. Fukutani, Effects of Rotational-Symmetry Breaking on Physisorption of Ortho- and Para-H_2on Ag(111), Phys. Rev. Lett. **112**, 146101 (2014).
[21] Y. Kunisada and H. Kasai, Hindered rotational physisorption states of H_2 on Ag(111) surfaces, Phys. Chem. Chem. Phys. **17**, 19625 (2015).
[22] J. A. Gupta, C. P Lutz, A. J. Heinrich, and D. M. Eigler, Strongly coverage-dependent excitations of adsorbed molecular hydrogen, Phys. Rev. B **71**, 115416 (2005).
[23] A. J. Therrien, A. Pronschinske, C. J. Murphy, E. A. Lewis, M. L. Liriano, M. D. Marcinkowski, and E. C. H. Sykes, Collective effects in physisorbed molecular hydrogen on Ni/Au(111), Phys. Rev. B **92**, 161407(R) (2015).
[24] S. Li, A. Yu, F. Toledo, Z. Han, H. Wang, H. Y. He, R. Wu, and W. Ho, Rotational and Vibrational Excitations of a Hydrogen Molecule Trapped within a Nanocavity of Tunable Dimension, Phys. Rev. Lett. **111**, 146102 (2013).
[25] F. D. Natterer, F. Patthey, and H. Brune, Distinction of Nuclear Spin States with the Scanning Tunneling Microscope, Phys. Rev. Lett. **111**, 175303 (2013).
[26] F. D. Natterer, F. Patthey, and H. Brune, Resonant-enhanced spectroscopy of molecular rotations with a scanning tunneling microscope, ACS Nano **8**, 7099(2014).
[27] S. Li, D. Yuan, A. Yu, G. Czap, R. Wu, and W. Ho, Rotational Spectromicroscopy: Imaging the Orbital Interaction Between Molecular Hydrogen and an Adsorbed Molecule, Phys. Rev. Lett. **114**, 206101 (2015).
[28] H. Wang, S. Li, H. He, A. Yu, F. Toledo, Z. Han, W. Ho, and R. Wu, Trapping and characterization of a single hydrogen molecule in a continuously tunable nanocavity, J. Phys. Chem. Lett. **6**, 3453 (2015).
[29] B. N. J. Persson, Inelastic Electron Tunneling from a Metal Tip: The Contribution from Resonant Processes, Phys. Rev. Lett. **59**, 339 (1987).
[30] N. Lorente and M. Persson, Theory of Single Molecule Vibrational Spectroscopy and Microscopy, Phys. Rev. Lett. **85**, 2997 (2000).
[31] A. Gagliardi, G. C. Solomon, A. Pecchia, T. Frauenheim, A. D. Carlo, N. S. Hush, and J. R. Reimers, *A priori* method for propensity rules for inelastic electron tunneling spectroscopy of single-molecule conduction, Phys. Rev. B **75**, 174306 (2007).
[32] H. Ueba, T. Mii, and S. Tikhodeev, Theory of inelastic tunneling spectroscopy of a single molecule—Competition between elastic and inelastic current, Surf. Sci. **601**, 5220 (2007).

[33] A. Troisi, M. A. Ratner, and A. Nitzan, Vibronic effects in off-resonant molecular wire conduction, J. Chem. Phys. **118**, 6072 (2003).

[34] M. Paulsson, T. Frederiksen, H. Ueba, N. Lorente, and M. Brandbyge, Unified Description of Inelastic Propensity Rules for Electron Transport Through Nanoscale Junctions, Phys. Rev. Lett. **100**, 226604 (2008).

[35] See Supplemental Materials at http://link.aps.org/supplemental/10.1103/PhysRevB.96.241409 for basic concepts of hydrogen nuclear-spin isomers, contribution of off-resonant and resonant electron tunneling, ΔM rotational selection rules, contribution of IET processes mediated by positive and negative ions, details of the nearly-free flexible-rotator model, details of DFT calculations, how to extract isotropic and anisotropic contributions of V and ΔR_e, trapping state of *para*-H_2 ($J = 0$) in V_0, contribution of quadrupole interaction on the potential anisotropy, rotational-energy shifts of two hydrogen molecules in nanocavity, and materials and methods, which includes Refs. [42–58].

[36] N. D. Lang, Vacuum Tunneling Current from an Adsorbed Atom, Phys. Rev. Lett. **55**, 230 (1985).

[37] G. D. Scholes and K. P. Chiggino, Electronic interactions and interchromophore excitation transfer, J. Phys. Chem. **98**, 4580 (1994).

[38] M. B. Smith and J. Michl, Recent advances in singlet fission, Annu. Rev. Phys. Chem. **64**, 361 (2013).

[39] S. M. Blinder, Dipole moment of HD, J. Chem. Phys. **32**, 105 (1960).

[40] C. P. Goncalves and J. R. Mohallem, Point group symmetries of the molecular orbitals of HD^+ beyond the Born–Oppenheimer approximation, Chem. Phys. Lett. **367**, 533 (2003).

[41] L. Wilzén, F. Althoff, S. Andersson, and M. Persson, Anisotropy of the physisorption interaction between H_2 and metal surfaces, Phys. Rev. B **43**, 7003 (1991).

[42] G. Herzberg, *Molecular Spectra and Molecular Structure* (Van Nostrand Reinhold, New York, 1939).

[43] H. L. Skriver and N. M. Rosengaard, Surface energy and work function of elemental metals, Phys. Rev. B **46**, 7157 (1992).

[44] T. E. Sharp, Potential-energy curves for molecular hydrogen and its ions, At. Data Nucl. Data Tables **2**, 119 (1971).

[45] K. Niki, T. Kawauchi, M. Matsumoto, K. Fukutani, and T. Okano, Mechanism of the *ortho-para* conversion of hydrogen on Ag surfaces, Phys. Rev. B **77**, 201404 (2008).

[46] G. J. Schulz, Resonances in electron impact on diatomic molecules, Rev. Mod. Phys. **45**, 423 (1973).

[47] K. Svensson and S. Andersson, Desorption of H_2, HD, and D_2 through Temporary Negative ion Formation, Phys. Rev. Lett. **109**, 196102 (2012).

[48] D. L. Mills, J. X. Cao, and R. Wu, Interaction of adsorbates with electric-field fluctuations near surfaces: Nonradiative lifetimes and energy-level shifts, Phys. Rev. B **75**, 205439 (2007).

[49] L. Gross, N. Moll, F. Mohn, A. Curioni, G. Meyer, F. Hanke, and M. Persson, High-Resolution Molecular Orbital Imaging Using a *p*-wave STM tip, Phys. Rev. Lett. **107**, 086101 (2011).

[50] A. Garcia-Lekue, D. Sanchez-Portal, A. Arnau, and T. Frederiksen, Simulation of inelastic electron tunneling spectroscopy of single molecules with functionalized tips, Phys. Rev. B **83**, 155417 (2011).

[51] G. Cilpa, M. Guitou, and G. Chambaud, Theoretical study of chemi- and physisorption processes of H_2 molecules on a (100) surface of silver, Surf. Sci. **602**, 2894 (2008).

[52] J. D. Poll and L. Wolniewicz, The quadrupole moment of the H_2 molecule, J. Chem. Phys. **68**, 3053 (1978).

[53] E. L. Koo, Electric field and energy of a point electric charge between confocal hyperboloidal electrodes, Rev. Mex. Fis. **47**, 303 (2001).

[54] D. R. Bates, K. Ledsham, and A. L. Stewart, Wave functions of the hydrogen molecular ion, Philos. Trans. R. Soc. London A **246**, 215 (1953).

[55] G. Kresse and J. Furthmüller, Efficient iterative schemes for *ab initio* total-energy calculations using a plane-wave basis set, Phys. Rev. B **54**, 11169 (1996).

[56] G. Kresse and D. Joubert, From ultrasoft pseudopotentials to the projector augmented-wave method, Phys. Rev. B **59**, 1758 (1999).

[57] I. Hamada, Van der Waals density functional made accurate, Phys. Rev. B **89**, 121103(R) (2014).

[58] H. J. Monkhorst and J. D. Pack, Special points for Brillouin-zone integrations, Phys. Rev. B **13**, 5188 (1976).